Journal of Solid State Chemistry 181 (2008) 2877–2881

Contents lists available at ScienceDirect

Journal of Solid State Chemistry

journal homepage: www.elsevier.com/locate/jssc

Quantum chemical study and low-temperature calorimetry of phase transition in $V_4S_9Br_4$

S.G. Kozlova [a,b,*], S.P. Gabuda [a], G.A. Berezovskii [a], D.P. Pischur [a], Y.V. Mironov [a], A. Simon [c], V.E. Fedorov [a]

[a] Nikolaev Institute of Inorganic Chemistry SB RAS, Novosibirsk 630090, Russian Federation
[b] Boreskov Institute of Catalysis SB RAS, Novosibirsk 630090, Russian Federation
[c] Max-Planck-Institut für Festkörperforschung, Heisenbergstraße 1, 70569 Stuttgart, Germany

ARTICLE INFO

Article history:
Received 8 February 2008
Received in revised form
24 June 2008
Accepted 14 July 2008
Available online 20 July 2008

Keywords:
Tetranuclear metal cluster
Phase transition
Electron localization function
Calorimetry

ABSTRACT

The phase transition in a mixed-valence tetranuclear compound $V_4S_9Br_4$ was studied by DFT calculations and low-temperature high-precision calorimetry. According to DFT data, the phase transition of the low-temperature modification may be accompanied by $C_{4v} \rightarrow C_{2v}$ symmetry lowering and electron spin pairing. A weak exchange-correlation interaction discovered between μ_4-S^{2-} and S^{2-} ions in $V_4S_9Br_4$ may play an important part in multicentered interactions. Experimental calorimetric data show that the phase transition is a displacive phase transformation.

© 2008 Elsevier Inc. All rights reserved.

1. Introduction

Metal cluster compounds are commonly regarded as promising objects for molecular electronics and for constructing nano-size materials. Vanadium thiobromide $V_4S_9Br_4$, a mixed-valence tetranuclear cluster compound, is one such material. It crystallizes in the tetragonal space group $P4/nmm$ ($a = 10.864$ Å, $c = 6.973$ Å) and is characterized as a paramagnetic high-spin cluster above 50 K and as a low-spin cluster below this temperature [1]. However, the details of the phase transition still remain unclear. The aim of the work has been to study the possible electron rearrangements in the cluster on phase change.

2. Experimental and computational details

2.1. Sample preparation

A powder sample of the vanadium thiobromide $V_4S_9Br_4$ was synthesized by the reaction of the elements in the ratio V:S:Br = 4:9:4 in an evacuated and sealed silica tube [1]. The tube was heated to 450 °C at the rate of 10 °C/h, kept at the temperature for 3 days, and then cooled at the rate of 20 °C/h till room temperature. The reaction product was washed with acetone and dried in vacuum. The X-ray powder diffraction pattern of the bulk sample is in perfect agreement with the pattern calculated for a single-crystal structure.

2.2. Theoretical approach

The electronic structure and the distribution of electronic density in the cluster fragments $[V_4S_9Br_8]^{4-}$ (Fig. 1 as a part of the polymeric network $V_4S_9Br_4$) was studied for C_{4v}, C_{2v}, and C_s symmetries. The C_{4v} symmetry conforms to a high-temperature state of vanadium thiobromide with the tetragonal space group $P4/nmm$ [1], while the C_{2v} and C_s symmetries are associated with a hypothetical low-temperature structure. The electronic structure and optimized distances of the models were obtained by spin-restricted density functional calculations (DFT) using the ADF2006 code [2] and widely used VWN & Becke & Perdew [3–5] and B3LYP [6] functionals. An STO/ZORA/TZP (and TZ2P) all-electron basis set was chosen for all atoms, where TZP and TZ2P are triple zeta basis sets with one and two polarization functions, respectively. The ZORA (zeroth-order relativistic approximation) method was used to account for the scalar relativistic effects [7]. The convergence criteria were set according to default values recommended by the designers of ADF2006. The electronic bonding energy of the model complexes was calculated according to the method [8,9] realized in the ADF2006 code. The electron density was studied by the topological method of the electron

* Corresponding author at: Nikolaev Institute of Inorganic Chemistry SB RAS, Lavrentieva, 3 Novosibirsk 630090, Russian Federation.
E-mail address: sgk@che.nsk.su (S.G. Kozlova).

0022-4596/$ - see front matter © 2008 Elsevier Inc. All rights reserved.
doi:10.1016/j.jssc.2008.07.013

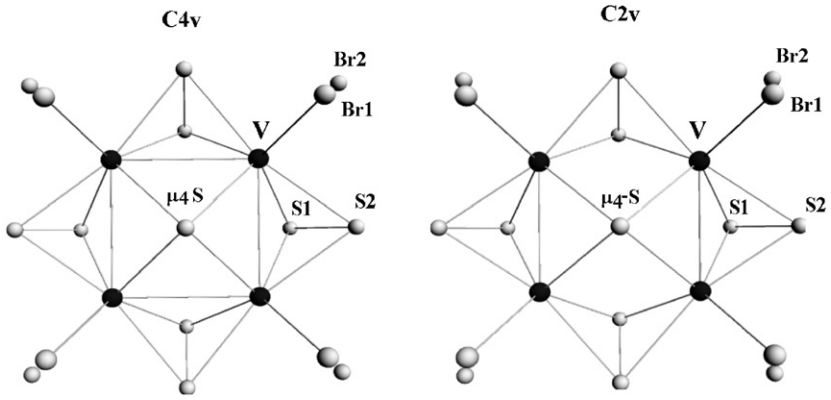

Fig. 1. Fragment $[V_4S_9Br_8]^{4-}$ of the crystal structure $V_4S_9Br_4$ with symmetry C_{4v} (left) and C_{2v} (right).

localization function (ELF) that appears to be a good tool to study chemical bonding [10–13]. The calculated ELF density was visualized using the ADFView program at a grid spacing of 0.05 Å; the integration of ELF values was carried out using the program Dgrid-4.1 [14].

2.3. Calorimetric measurements

The isobar thermal capacity C_p of $V_4S_9Br_4$ was measured on a vacuum adiabatic calorimeter with periodic heat input in an interval of 8.6–308 K at 64 points (Table 1). The $V_4S_9Br_4$ polycrystalline sample of the mass 1.5208 g (or 0.001873 mol) was placed in a nickel calorimetric ampoule. The temperature of the ampoule was measured by a platinum resistance thermometer. The technique was calibrated against the capacity of benzoic acid. The deviation from the standard C_p values of benzoic acid was ~1.0% at 7–30 K, and the accuracy was 0.1–0.2% in the intervals 50–270 K. The entropy contributions due to anomalies can be inferred from the regular behavior of C_p(reg) in the absence of the anomalies. We approximated the regular C_p(reg) by a ninth-degree polynomial. The polynomial dependence C_p(reg) describes the experimental behavior of $C_p(T)$ to a good accuracy in the intervals 18–37 K (0.52%) and 70–107 K (0.65%).

Table 1
Experimental thermal capacity C_p ($J\,mol^{-1}\,K^{-1}$) of $V_4S_9Br_4$

T (K)	C_p	T (K)	C_p	T (K)	C_p	T (K)	C_p
8.60	8.507	26.18	44.26	89.86	212.2	173.80	327.7
9.66	11.04	27.46	47.88	90.37	217.3	180.34	333.5
10.61	13.30	29.59	54.18	92.44	217.4	190.00	344.7
11.57	16.69	33.04	63.96	95.18	225.3	198.81	352.0
12.64	21.44	37.30	78.01	95.77	222.1	207.45	360.1
13.69	28.37	42.14	93.12	101.31	235.1	215.27	366.6
14.62	36.49	47.48	118.1	107.04	243.9	223.38	377.7
16.00	32.90	53.12	134.6	112.51	254.8	238.62	391.5
17.21	26.33	58.94	143.2	118.54	262.9	246.86	399.0
18.32	27.34	64.93	154.8	125.31	275.2	254.97	403.4
19.33	28.94	71.33	171.3	132.67	284.2	262.97	408.8
20.43	31.06	80.85	190.1	143.00	294.0	279.08	416.1
21.60	33.50	81.49	195.1	148.74	301.2	295.33	419.7
22.75	35.83	84.40	200.7	154.84	310.6	299.43	421.1
23.87	38.58	85.19	200.7	160.82	313.7	303.57	424.7
25.04	41.85	87.18	208.6	167.13	322.8	307.61	427.5

Table 2
Geometric parameters for $[V_4S_9Br_8]^{4-}$ with C_{4v} symmetry calculated with different DFT functionals and basis sets and experimental data

Functional	VWN & Becke & Perdew		B3LYP		Experiment
Basis	TZP	TZ2P	TZP	TZ2P	[1]
Bond (Å)					
V–V	2.916	2.913	2.831	2.821	3.005
V–μ_4-S	2.427	2.424	2.375	2.366	2.373
S1–S2	2.062	2.057	2.042	2.025	2.023
V–S1	2.388	2.386	2.336	2.330	2.392
V–S2	2.367	2.365	2.315	2.308	2.382
V–Br1	2.607	2.604	2.530	2.521	2.597
V–Br2	2.886	2.880	2.710	2.692	2.613
Angle of the bond (deg)					
V–μ_4-S–V	73.8	73.9	73.2	73.2	78.6
V–S1–V	75.3	75.3	74.6	74.5	77.8
V–S2–V	76.0	76.0	75.4	75.3	78.2
Br1–V–Br2	86.1	86.0	86.0	85.9	85.0

Symbols are the same as in Fig. 1.

3. Results

3.1. DFT calculations

Table 2 shows the interatomic optimized and computed distances in the $[V_4S_9Br_8]^{4-}$ complexes with C_{4v} symmetry. The geometric parameters closest to the experimental data were obtained with the functionals [3–5]. The discrepancy between the computed and experimental data may be due to the chosen model since an isolated cluster hardly can provide a faithful description of a real polymeric compound. Calculation data of $[V_4S_9Br_8]^{4-}$ vibration spectra indicate a single imaginary frequency 6.97 cm^{-1} with zero dipole strength. A vibration with a near-zero frequency cannot possibly have any considerable effect on the stability of the chosen model; moreover, it can be explained merely by the computational accuracy. Therefore we believe that the result proves the chosen system to be a rather accurate model.

Table 3 shows the optimized bonding energies of the complexes $[V_4S_9Br_8]^{4-}$ with C_{4v}, C_{2v}, and C_S symmetries as a result of DFT calculations according to the method from [8,9]. The C_{2v} and C_S complexes were found to be associated with lower bonding energies than the C_{4v} complexes, irrespective of the chosen functionals and basis sets, and the energy gain made 0.2–0.3 eV. Note that the C_{2v} and C_S symmetries have similar formation energies. Table 4 shows the optimized V–V distances of the hypothetical complexes $[V_4S_9Br_8]^{4-}$ with C_{2v} symmetry (Fig. 1). The optimized distances between interacting atoms in $[V_4S_9Br_8]^{4-}$ with the C_S and C_{2v} symmetries were similar as well: for example, the torsion angle V–V–V–V was only 0.1°, the V–V distances were 2.702, 3.121, 2.700, and 3.111 Å, the V–μ_4-S

Table 3
Bonding energies for $[V_4S_9Br_8]^{4-}$ systems with C_{4v}, C_{2v}, and C_S symmetries calculated with different DFT functionals and basis sets

C_{4v}				C_{2v}				C_S			
VWN & Becke Perdew		B3LYP		VWN & Becke Perdew		B3LYP		VWN & Becke Perdew		B3LYP	
TZP	TZ2P	TZP	TZ2P	TZP	TZ2P	TZP	TZ2P	TZP	TZ2P	TZP	TZ2P
−91.7	−93.0	−105.4	−106.9	−91.9	−93.3	−105.6	−107.2	−91.9	−93.2	−105.6	−107.2

Table 4
Geometric parameters for $[V_4S_9Br_8]^{4-}$ with C_{2v} symmetry calculated with different DFT functionals and basis sets

Functional	VWN & Becke & Perdew		B3LYP	
Basis	TZP	TZ2P	TZP	TZ2P
Bond (Å)				
V–V	2.688; 3.106	2.678; 3.102	2.631; 3.023	2.626; 3.024
V–μ_4-S	2.438	2.428	2.376	2.373
S1–S2	2.053; 2.070	2.037; 2.055	2.028; 2.046	2.010; 2.028
V–S1	2.355; 2.417	2.349; 2.412	2.317; 2.358	2.311; 2.357
V–S2	2.358; 2.383	2.344; 2.374	2.307; 2.329	2.299; 2.323
V–Br1	2.607	2.596	2.526	2.509
V–Br2	2.925	2.903	2.722	2.701
Angle of bond (deg)				
V–μ_4-S–V	66.9; 79.1	66.9; 79.4	67.2; 79.0	67.2; 79.2
V–S1–V	69.6; 80.0	69.5; 80.0	69.2; 79.7	69.2; 79.8
V–S2–V	69.5; 81.4	69.7; 81.6	69.6; 80.9	69.7; 81.2
Br1–V–Br2	86.1	86.0	86.2	86.1

Symbols are the same as in Fig. 1.

distances were 2.422, 2.435, 2.439, and 2.429 Å (with [3–5] functionals and TZP basis). Therefore, the phase transition at 14.5 K may be interpreted as a phase transition with the $C_{4v} \rightarrow C_{2v}$ (or pseudo C_{2v}) symmetry reduction. Figs. 2a and b show the molecular levels and the molecular orbitals (MOs) of complex $[V_4S_9Br_8]^{4-}$ with the C_{4v} and C_{2v} symmetries (C_{2v} is considered for the sake of simplicity) and the symmetry transformation of MOs at the $C_{4v} \rightarrow C_{2v}$ symmetry reduction. The highly symmetrical structure C_{4v} corresponds to a paramagnetic state and is characterized by a Jahn–Teller effect (the doubly degenerate 65E level is occupied by 2 electrons). The magnetic behavior of the $V_4S_9Br_4$ system was previously studied in [1]. The low symmetrical structure C_{2v} corresponds to a diamagnetic state. The shapes of the MOs indicate an increase in paired interaction between vanadium atoms in the low symmetrical structure C_{2v}.

The V–V interactions were studied by considering the electron density of $[V_4S_9Br_8]^{4-}$ using the ELF method. In the paramagnetic C_{4v} system the valence electrons of the vanadium atoms are strongly delocalized and are imaged by the areas ELF≈0.25 between V atoms in contrast to the short V–V bonds in the C_{2v} structure with clearly visible bonding disynaptic basins of electron spin pairing (Figs. 3 and 4). The area of electron localization was identified as a disynaptic basin by the Dgrid-4.1 program as well. ELF integration with [14] showed that the maximum ELF value in the disynaptic basins was 0.503.

Note that the disynaptic basins are displaced towards the μ_4-S^{2-} ion rather than lying on the V–V line. This may be caused by their interactions with sulfur atoms in the S_2^{2-} and μ_4-S^{2-} anions. The μ_4-S^{2-} and S_2^{2-} anions are connected with each other by a binding path in the C_{4v} symmetry system (ELF∼0.3, Figs. 3(1) and 5). In the C_{2v} system, the path between μ_4-S^{2-} and S_2^{2-} anions is present only in the area of disynaptic basins (Figs. 4(1) and 5).

The interactions between μ_4-S^{2-} and V and monosynaptic basins of S atoms do not change from the ELF viewpoint (Figs. 3(2) and 4(2)).

3.2. Calorimetric data

The measurements of the structural properties of $V_4S_9Br_4$ below 15 K could provide the most direct confirmation of the suggested phase transition model. However, our efforts to run the experiment failed due to the behavior of the crystals, which cracked and crumbled in the vicinity of the phase transition.

The thermal capacity of $V_4S_9Br_4$ was measured with a high-precision adiabatic calorimetric technique to refine the thermodynamic characteristics [1]. Fig. 6 shows the isobar thermal capacity C_p of $V_4S_9Br_4$. It also shows an anomaly with its peak at 14.6 K, a diffuse anomaly at 35–70 K, and a high scatter (up to 4%) of the experimental points at 80–100 K. The excess enthalpy, ΔH, and the entropy of transitions, ΔS, were determined for the intervals 8.6–20 K and 35–71 K by subtraction of the C_p(reg) from C_p. The results of ΔH and ΔS calculations are presented in Table 5.

The low-temperature anomaly (at 14.6 K) corresponds to a displacive phase transition since ΔS is less than $R \ln 2$. The diffuse anomaly (35–70 K with a maximum at ∼50 K) correlates with the abnormal behavior of magnetic susceptibility near 50 K and may be associated with the terminal excitation of electrons [1]. The high scattering of the experimental points at 80–100 K apparently reflects some fluctuation effects in the vicinity of the anomaly.

4. Discussion and conclusions

According to the reported precision measurements of heat capacity, the phase transition observed in vanadium thiobromide $V_4S_9Br_4$ at ∼15 K is a displacive phase transition. The heat anomaly in the area of phase transition is shown to peak at 50 K. The anomaly correlates with a magnetic susceptibility anomaly associated with the occurrence of paramagnetic properties in $V_4S_9Br_4$. Unfortunately, we failed to discover this effect before when measuring the heat capacity on a scanning calorimeter [1].

According to DFT data, the displacive phase transition can be explained by the displacement of vanadium atoms associated with the formation of a phase with the C_{2v} (or pseudo C_{2v}) symmetry.

The presence of V–V disynaptic basins can possibly indicate that the phase transition is associated with electron pairing (paramagnetic–diamagnetic phase transition). This interpretation is supported by experimental magnetic measurements [1]. Low ELF values (∼0.503) are a special feature of these attractors. Rather low values of valent attractors for *d* element clusters were also reported before, for example, for Fe_4 clusters (ELF = 0.438) [15] and for Cu fcc lattice (ELF = 0.2) [16] and are explained by the fact that electron localization is greatly reduced due the Pauli repulsion exerted by the electron density concentrated in core regions. We believe that this explanation works also in our case. Another peculiarity of the discovered attractors is that they do not lie on the V–V line and slightly interact with μ_4-S^{2-} and S_2^{2-} anions in the C_{2v} system. However, the results of mathematical processing with program [14] indicated the presence of

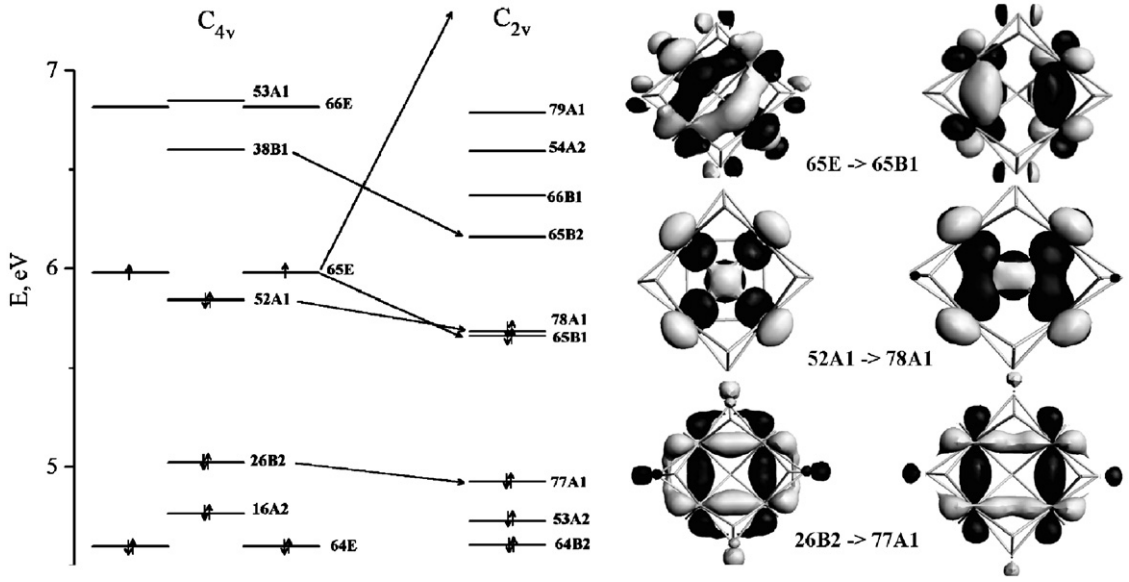

Fig. 2. MO levels in $[V_4S_9Br_8]^{4-}$ with C_{4v} and C_{2v} symmetries, level correlation depicted with arrows (left) and molecular orbitals of $[V_4S_9Br_8]^{4-}$ (right).

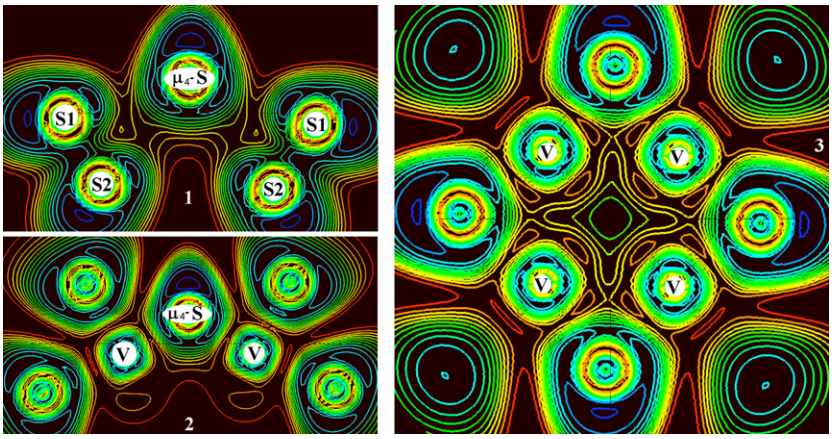

Fig. 3. ELF distribution in the V_4 plane of the $[V_4S_9Br_8]^{4-}$ system with C_{4v} symmetry. S1–μ_4-S–S1 plane (1); V–μ_4-S–V plane (2); V–V–V–V plane (3). Blue color shows ELF→1, red color shows ELF→0.

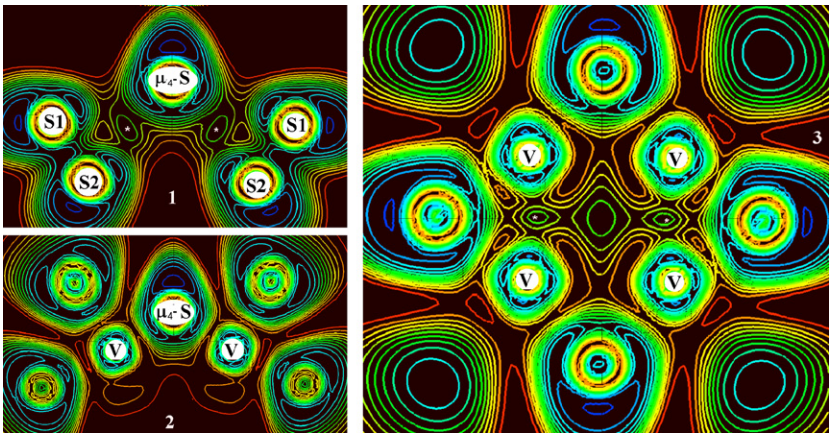

Fig. 4. ELF distribution in the V_4 plane of the $[V_4S_9Br_8]^{4-}$ system with C_{2v} symmetry. S1–μ_4-S–S1 plane containing C_2 axis (1); V–μ_4-S–V plane containing C_2 axis (2); V–V–V–V plane (3). *Depicted the disynaptic basins of electron pairs between V atoms. Blue color shows ELF→1, red color shows ELF→0.

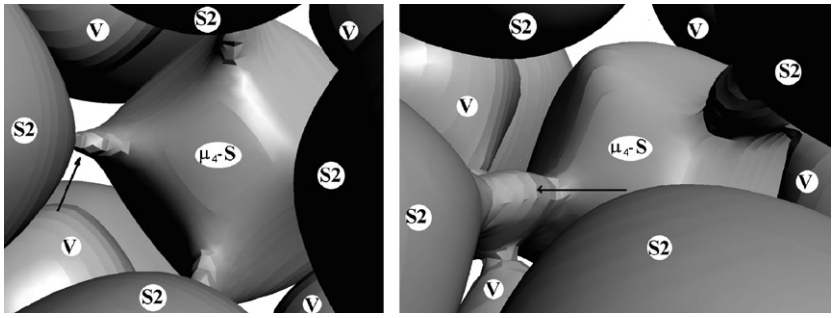

Fig. 5. Isosurfaces ELF = 0.3 for $[V_4S_9Br_8]^{4-}$ structures with C_{4v} (right) and C_{2v} (left) symmetries. Arrows depicted the bonding path between μ_4-S^{2-} and S_2^{2-} for C_{2v} symmetry and the bonding path between μ_4-S^{2-} and S_2^{2-} with disynaptic basin between V for C_{4v} symmetry.

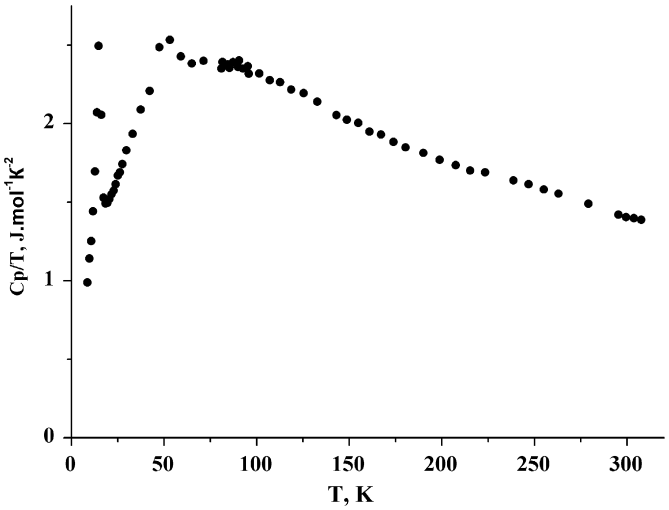

Fig. 6. Temperature dependence of thermal capacity C_p (from Table 1) plotted in the C_p/T coordinates to magnify the anomalies.

Table 5
Experimental thermodynamic data for $V_4S_9Br_4$

Intervals (K)	8.6–20	37–71
ΔH ($J\,mol^{-1}$)	61 ± 6	340 ± 30
ΔS ($J\,mol^{-1}\,K^{-1}$)	4.3 ± 0.4	6.6 ± 0.7

disynaptic basins only, again μ_4-S^{2-}–V–S_2^{2-} bonding paths are visually associated with ELF∼0.3. Therefore we conclude that the interactions between V atoms and μ_4-S^{2-} and S_2^{2-} anions are weak as compared with V–V interactions.

Nevertheless, the interactions between μ_4-S^{2-} and S_2^{2-} ions in the C_{4v} structure and μ_4-S^{2-}–V–S_2^{2-} in the C_{2v} structure proved by the presence of bonding paths can be described as exchange–correlation interactions or, in other words, as a special type of weak closed shell interactions. These interactions may presumably play an important part in the stability of $V_4S_9Br_4$ and its properties.

Bonding attractors are found between two V atoms at a distance of 2.69 Å, which is close to the short V–V distances in VO_2 (2.62 Å [17]). The structural phase transition in VO_2 is known to be accompanied by the change of its metallic properties (metal-to-semiconductivity phase transition) [17–19]. Crystals of $V_4S_9Br_4$ never demonstrate metallic properties at room temperature, so the change in their magnetic properties is of theoretical interest by itself.

Acknowledgments

The study was supported by RFBR 08-03-00826, RFBR- Ukraine 08-03-90413-Ukr_a and Taiwan National Science Council (Grants 06-03-89503-HHC and 95WFD0300050/Contract no. RP06N02-2).

References

[1] Yu.V. Mironov, S.S. Yarovoi, D.Y. Naumov, S.G. Kozlova, V.N. Ikorskii, R.K. Kremer, A. Simon, V.E. Fedorov, J. Phys. Chem. B 109 (2005) 23804–23807.
[2] Amsterdam Density Functional (ADF) program, Release 2006.02, Vrije Universteit, Amsterdam, The Netherlands, 2006.
[3] S.H. Vosko, L. Wilk, M. Nusair, Can. J. Phys. 58 (1980) 1200–1211.
[4] A.D. Becke, Phys. Rev. A 38 (1988) 3098–3100.
[5] J.P. Perdew, Phys. Rev. B 33 (1986) 8822–8824.
[6] P.J. Stephens, F.J. Devlin, C.F. Chabalowski, M.J. Frisch, J. Phys. Chem. 98 (1994) 11623–11627.
[7] E. van Lenthe, A.E. Ehlers, E.J. Baerends, J. Chem. Phys. 110 (1999) 8943–8953.
[8] E.J. Baerends, V. Branchadell, M. Sodupe, Chem. Phys. Lett. 265 (1997) 481–489.
[9] T. Ziegler, A. Rauk, J. Theor. Chem. Acta 46 (1977) 1–10.
[10] M.G. Cory, M.C. Zerner, Chem. Rev. 91 (1991) 813–822.
[11] A. Savin, O. Jepsen, O.K. Flad, H. Andersen, H.G. von Schnering, Angew. Chem. 1 (1992) 187–188.
[12] B. Silvi, A. Savin, Nature 371 (1994) 683–686.
[13] D.L. Cooper, Nature 371 (1994) 651–652.
[14] M. Kohout, Program DGrid 4.1, Max Planck Institute for Chemical Physics of Solids, Dresden, 2006.
[15] S. Berski, G.L. Gutsev, M.D. Mochena, J. Andres, J. Phys. Chem. A 108 (2004) 6025–6031.
[16] B. Silvi, C. Gatti, J. Phys. Chem. A 104 (2000) 947–953.
[17] J.B. Goodenough, Progress in Solid State Chemistry, vol. 5, Pergamon, New York, 1974.
[18] L.A. Boyarskii, S.P. Gabuda, S.G. Kozlova, Physica B 284–288 (1–4) (2000) 1454–1455.
[19] J. Umeda, H. Kusumoto, K. Narita, E. Yamada, J. Chem. Phys. 42 (1965) 1458–1467.